PAPER

The construction of a heterostructured RGO/g-C₃N₄/LaCO₃OH composite with enhanced visible light photocatalytic activity for MO degradation†

Deng Gu,[ab] Yuanjin Wang,[a] Zhiman Liang,[a] Yanting Dou,[a] Zhenhe Xu, [iD] *[a] Jiqi Zheng,*[a] Yaguang Sun, [iD] [b] Fu Ding [iD] *[b] and Yu Gao*[a]

The construction of a heterojunction and the introduction of a cocatalyst can both promote the transfer of photogenerated electrons, which are effective strategies to enhance photocatalytic efficiency. In this paper, a ternary RGO/g-C₃N₄/LaCO₃OH composite was synthesized by constructing a g-C₃N₄/LaCO₃OH heterojunction and introducing a non-noble metal cocatalyst RGO through hydrothermal reactions. TEM, XRD, XPS, UV-vis diffuse reflectance spectroscopy, photo-electrochemistry and PL tests were carried out to characterize the structures, morphologies and carrier separation efficiencies of products. Benefiting from the boosted visible light absorption capability, reduced charge transfer resistance and facilitated photogenerated carrier separation, the visible light photocatalytic activity of the ternary RGO/g-C₃N₄/ LaCO₃OH composite was effectively improved, resulting in a much increased MO (methyl orange) degradation rate of 0.0326 min^{-1} compared with LaCO₃OH (0.0003 min^{-1}) and g-C₃N₄ (0.0083 min^{-1}). Moreover, by combining the results of the active species trapping experiment with the bandgap structure of each component, the mechanism of the MO photodegradation process was proposed.

1. Introduction

Environmental pollution is one of the main challenges for the rapid development of a green economy.[1] Photocatalysis based on semiconductors is considered as a promising technology with wide application prospects to address environmental problems.[2] However the development of photocatalysts with low cost, high stability and efficiency remains a challenge.[3] Though rare earth-based materials including YVO₄,[4] CeO₂ (ref. 5) and LaCO₃OH[6] have attracted wide attention in photocatalysis, their application is still limited because of their large bandgaps, leading to a poor ability in visible light absorption.[7] The construction of heterojunctions,[8,9] the introduction of cocatalysts[10] and elemental doping[11] are effective strategies to decrease the bandgaps of rare earth photocatalysts and hence improve the utilization efficiency of visible light and accelerate the kinetics of photocatalytic process.

LaCO₃OH is a rare earth hydroxyl carbonate with an excellent luminescence property, showing a great potential in photocatalytic pollutants degradation and H₂ evolution.[12,13] LaCO₃OH

[a]College of Environmental and Chemical Engineering, Dalian University, Dalian 116622, China. E-mail: xuzh@syuct.edu.cn; jiqizheng@yeah.net; gaoy777@126.com

[b]Key Laboratory of Inorganic Molecule-Based Chemistry of Liaoning Province, Shenyang University of Chemical Technology, Shenyang, 110142, China. E-mail: dingfu@syuct.edu.cn

has a relatively broad bandgap of 4.0 eV, which could inhibit the recombination of photogenerated carriers.[14] On the other side, as a result of the broad bandgap, it can only absorb ultraviolet light in photocatalytic reactions. Based on recent research, the visible light absorption capability of LaCO₃OH can be boosted by constructing heterojunction.[15] Under visible light irradiation, pure LaCO₃OH showed a negligible photocatalytic activity, while heterostructured g-C₃N₄/LaCO₃OH synthesized through a one-step hydrothermal reaction exhibited a substantially enhanced NO removal ratio of 30.3% after 30 min.[16] g-C₃N₄, a kind of semiconductor photocatalyst, has drawn wide attention in vast fields because of its visible light response and layered structure, which can provide rich surface chemistry and shorten the electron transfer pathways.[17] While there are only few reports about g-C₃N₄/LaCO₃OH heterojunction as the catalyst for the photodegradation of organic dyes at present. Wang et al.[13] synthesized a g-C₃N₄/LaCO₃OH heterostructure for photocatalytic NO removal, which showed an improved NO removal ratio of 30.3% compared with pristine g-C₃N₄ (19.3%) after 30 min visible light irradiation. Similar composite also shown considerable improvement in N₂ photofixation (8.2 mM g⁻¹ h⁻¹) compared to g-C₃N₄ (2.1 mM g⁻¹ h⁻¹).[18] While there is still no report about the application of g-C₃N₄/LaCO₃OH heterojunction in the photodegradation of dyes. The introduction of cocatalyst such as noble metal (Pt[19] and Ag[20]), non-noble metal (Ni[21]) and non-metal material such as graphene oxide (GO) can restrain the recombination of photogenerated carriers and enhance visible light absorption capacity.[22] Among all these

cocatalysts, GO has fascinating properties including good conductivity, high carrier mobility and large exposed specific surface, which can provide abundant active sites for the photocatalytic process.[23] Therefore, for the first time, we proposed to introduce reduced graphene oxide (RGO) into g-C_3N_4/LaCO$_3$OH heterojunction and result in a heterostructured ternary composite for photocatalytic degradation of the organic dye. Benefitting from the extended light absorption in visible light region along with accelerated separation kinetics of charge carriers, the constructed RGO/g-C_3N_4/LaCO$_3$OH composite can serve as the catalyst for the photodegradation of methyl orange (MO) under visible light irradiation with a superior performance than each component.

Herein, ternary composite RGO/g-C_3N_4/LaCO$_3$OH heterojunction was synthesized through hydrothermal reactions and its photocatalytic activity was evaluated by using it as the catalyst in the degradation of MO under visible light irradiation. The photocatalysis mechanism was investigated and the migration pathway of photogenerated carriers was proposed. This work is excepted to provide a novel strategy to enhance the photocatalytic activity of rare-earth based semiconductors with broad bandgaps for the photodegradation of organic dyes.

2. Experimental section

2.1 Materials

Analytical grade chemicals were used directly in the experiments. Graphite powder, $K_2S_2O_8$, H_2SO_4, HCl, $KMnO_4$ and $BaCl_2$ were purchased from Sinopharm, China. Urea, La(NO$_3$)$_3$·6H$_2$O and MO were provided by Aladdin, China.

g-C_3N_4 was synthesized through the method in the literature.[24] 10.0 g urea was calcined at 250 °C for 1 h, then 350 °C for 2 h and 550 °C for another 2 h in a tube furnace. The obtained pale yellow powder was washed with distilled water then dried at 60 °C for 12 h.

X wt% g-C_3N_4/LaCO$_3$OH (X represents the mass ratio of g-C_3N_4, X = 15.0, 25.0, 35.0) was synthesized through a hydrothermal reaction. For 15.0 wt% g-C_3N_4/LaCO$_3$OH, 50.0 mg g-

C_3N_4 and 671.6 mg La(NO$_3$)$_3$·6H$_2$O were dispersed in 35 mL distilled water and stirred for 3 h. After adjusting pH to 8.0–8.5 using 0.1 M NaOH aqueous solution, the obtained suspension was transferred to 100 mL autoclave and heated at 160 °C for 6 h. After washed with distilled water for 3 times, the product was dried at 60 °C for 12 h. Pure LaCO$_3$OH was also produced *via* a reported method for comparison.[14]

RGO/g-C_3N_4/LaCO$_3$OH was obtained through a hydrothermal reaction using g-C_3N_4/LaCO$_3$OH and GO as raw materials, as shown in Scheme 1, and the latter was produced by the Hummers' method.[10] For Y wt% RGO/g-C_3N_4/LaCO$_3$OH (Y represents the mass ratio of RGO, X = 0.6, 0.8, 1.0), 50.0 mg 25.0 wt% g-C_3N_4/LaCO$_3$OH was dispersed in 35.0 mL distilled water, in which 400.0 µL GO suspension (1.0 mg mL^{-1}) was added. The obtained mixture was heated at 160 °C for 6 h in an autoclave, and the product was washed and dried in the same way as the synthesis of g-C_3N_4/LaCO$_3$OH sample.

2.2 Characterization

An X-ray diffractometer (XRD, Bruker D8 Advance) with Cu Kα radiation was used to characterize the products' structures. X-ray photoelectron spectroscopy (XPS) was performed on Thermal ESCALAB 250Xi. The morphologies, microstructures, elemental mappings and the corresponding energy-dispersive X-ray spectroscopy (EDS) of the products were recorded by transmission electron microscopy (TEM, JEOL JEM 2010 EX). UV-vis diffuse reflectance spectra were tested on a Shimadzu UV-2500 spectrophotometer using BaSO$_4$ as the reference. Photoluminescence spectra (PL) were characterized by a F4500 Hitachi spectrophotometer with an excitation wavelength of 330 nm. The photoelectrochemical performance and electrochemical impedance spectroscopy (EIS) of the products were performed on a CHI 660E workstation using a three electrode system in 0.2 M Na$_2$SO$_4$ aqueous solution. The counter electrode was Pt wire and the reference electrode was saturated calomel electrode. For the working electrode, 10 mg product was dispersed in 1.0 mL ethanol and the suspension was dropped on fluorine-doped tin oxide (FTO) glass.
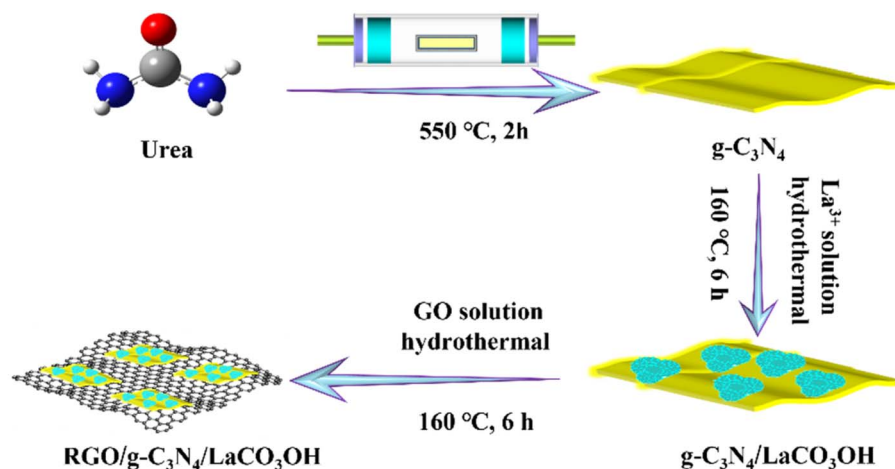
Scheme 1 The schematic fabrication process of RGO/g-C_3N_4/LaCO$_3$OH composite.

2.3 Photocatalytic tests

Photocatalytic performances of the obtained products were evaluated through the degradation of MO under visible light irradiation ($\lambda > 420$ nm), which was provided by a Xe lamp with a filter. The photograph of the lamp and the transmission spectrum of the filtered light were shown in Fig. S1.† 10 mg sample and 20 mL MO solution (10 mg L^{-1}) was added in to a quartz reactor, whose temperature was maintained at 30 °C. After stirring in darkness for 1 h to establish the adsorption–desorption equilibrium, the suspension was exposed in visible light. The concentrations of MO under different irritation times were then calculated based on the intensities of the peak at 465 nm in UV-vis spectra.

3. Results and discussion

As shown in Scheme 1, ternary RGO/g-C$_3$N$_4$/LaCO$_3$OH hetero-junction was synthesized through a two-step hydrothermal process. It can be observed in Fig. 1A that the synthesized g-C$_3$N$_4$ composes of 2D nanosheets with smooth and uniform surface. g-C$_3$N$_4$/LaCO$_3$OH heterojunction was fabricated by the *in situ* growth of LaCO$_3$OH on the surface of g-C$_3$N$_4$ *via* the hydrothermal reaction. In this process, g-C$_3$N$_4$ served as a self-sacrificial agent to produce CO$_3^{2-}$ and OH$^-$ due to the weaker binding energy of C chain. Then La^{3+} ions adsorbed on g-C$_3$N$_4$ reacted with the generated CO$_3^{2-}$ and OH$^-$ to produced LaCO$_3$OH, resulting in the *in situ* construction of g-C$_3$N$_4$/LaCO$_3$OH heterojunction.[13,18] The TEM image (Fig. 1B) shows that LaCO$_3$OH nanoparticles with diameters of 20–50 nm are evenly dispersed on g-C$_3$N$_4$. Then RGO was further introduced as the cocatalyst to obtain ternary RGO/g-C$_3$N$_4$/LaCO$_3$OH (Fig. 1C). In the high-resolution TEM image, the heterostructure interface between the (3 0 0) plane of LaCO$_3$OH and (0 0 2) plane of g-C$_3$N$_4$ can be clearly observed (Fig. 1D), suggesting the construction of g-C$_3$N$_4$/LaCO$_3$OH heterojunction. The scanning TEM image, corresponding elemental mappings and EDS
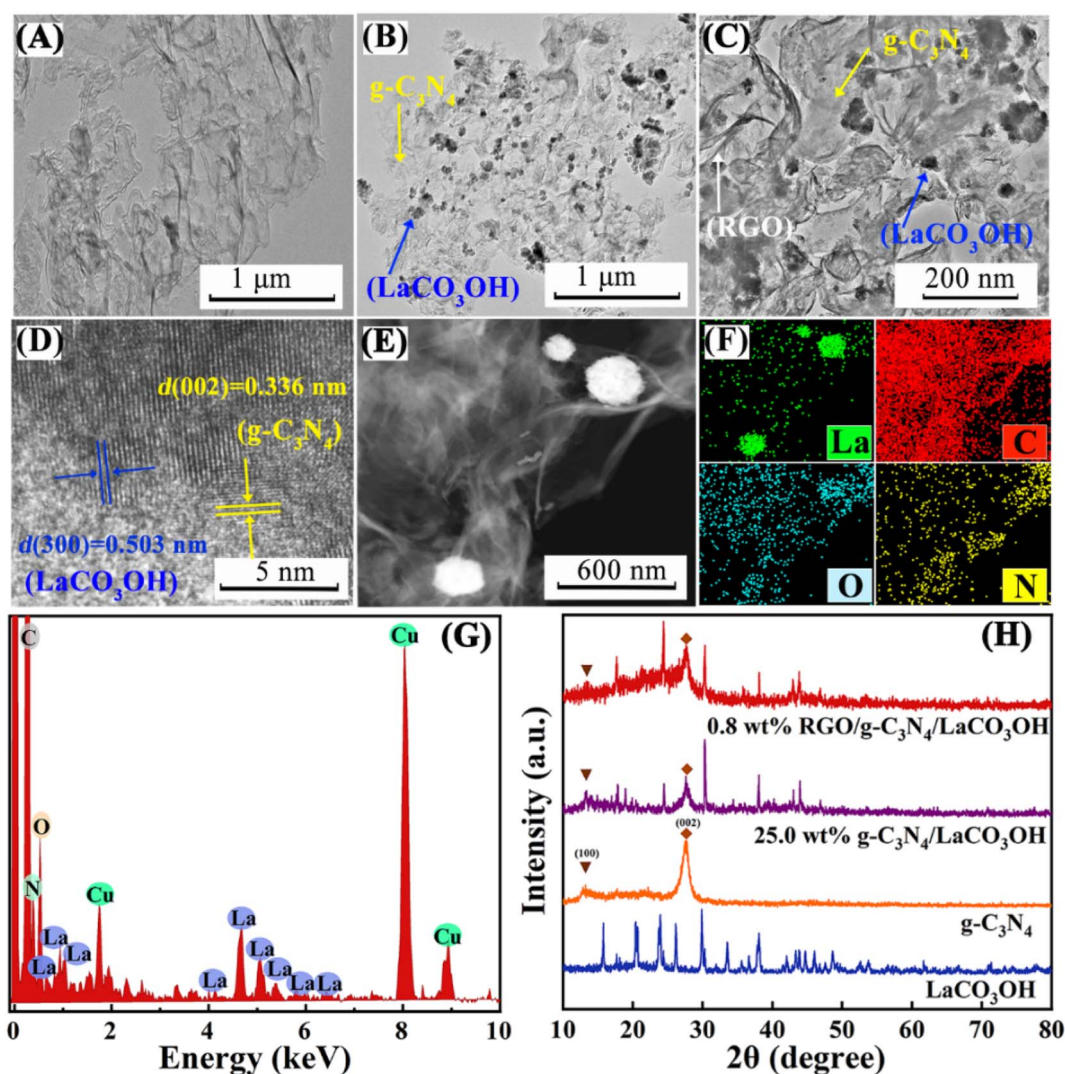

Fig. 1 TEM images of (A) g-C$_3$N$_4$, (B) g-C$_3$N$_4$/LaCO$_3$OH and (C) RGO/g-C$_3$N$_4$/LaCO$_3$OH; a high-resolution TEM image (D), a scanning TEM image (E), the corresponding elemental mappings (F) and the EDS spectrum (G) of RGO/g-C$_3$N$_4$/LaCO$_3$OH; (H) XRD patterns of LaCO$_3$OH, g-C$_3$N$_4$, g-C$_3$N$_4$/LaCO$_3$OH and RGO/g-C$_3$N$_4$/LaCO$_3$OH.

spectrum (Fig. 1E–G) verify that RGO/g-C$_3$N$_4$/LaCO$_3$OH are composed of La, C, O and N element, and La mainly distributed in the nanoparticles, which is consistent with the TEM results. The XRD patterns of LaCO$_3$OH, g-C$_3$N$_4$, g-C$_3$N$_4$/LaCO$_3$OH and RGO/g-C$_3$N$_4$/LaCO$_3$OH are shown in Fig. 1H. For the synthesized LaCO$_3$OH, its XRD pattern agrees well with hexagonal LaCO$_3$OH (JCPDS No. 49-0981).[14] In the XRD pattern of g-C$_3$N$_4$, two typical peaks at 13.20° and 27.54° are corresponding to the (1 0 0) and (0 0 2) plane, respectively.[16] The typical peaks of both LaCO$_3$OH and g-C$_3$N$_4$ can be observed in the g-C$_3$N$_4$/LaCO$_3$OH and RGO/g-C$_3$N$_4$/LaCO$_3$OH composite with good crystallinities, indicating that the crystal structures of these two components were maintained during the hydrothermal processes. With the introduction of RGO, the (0 0 2) peak of g-C$_3$N$_4$ broaden because of the interlayer stacking between 2D RGO and g-C$_3$N$_4$ sheets.[25] All the above results clarified that ternary RGO/g-C$_3$N$_4$/LaCO$_3$-OH heterojunction was successfully constructed.

XPS spectra are used to further study the constitution and surface chemical states of the products. In the survey spectrum of RGO/g-C$_3$N$_4$/LaCO$_3$OH (Fig. 2A), La, C, O and N elements can be identified, which is in accordance with the results of EDS. As shown in Fig. 2B, the spectrum of La 3d can be divided into two pairs of peaks. Peaks at 851.9 and 835.1 eV can be assigned to La 3d$_{3/2}$ and 3d$_{5/2}$ of La^{3+}, respectively, and peaks at 855.5 and 838.5 eV are two corresponding shakeup satellite peaks.[14] C 1s spectrum of RGO/g-C$_3$N$_4$/LaCO$_3$OH can be fitted into five peaks

considering three different sources (Fig. 2C). Peaks at 286.4, 285.1 and 286.4 eV can be indexed to O–C–O, C–OH and C–C in RGO, respectively. Peaks at 289.2 and 288.3 eV stem from CO$_3^{2-}$ in LaCO$_3$OH and N–C=N in g-C$_3$N$_4$, respectively. Compared with g-C$_3$N$_4$, the binding energy of N–C=N in RGO/g-C$_3$N$_4$/LaCO$_3$OH increased by 0.3 eV because of the electron transfer at the interfaces of the composite.[6] For N 1s spectrum, peaks at 400.8, 399.4 and 398.5 eV are attributed to C–N–H (or C–NH$_2$), N–C and N=C–N in g-C$_3$N$_4$, respectively (Fig. 2D).[17] The groups such as –OH and –NH$_2$ can provide abundant active sites for the photodegradation of MO.

UV-vis spectra of LaCO$_3$OH and g-C$_3$N$_4$ were measured to evaluate their band gap structures (Fig. 3A). The light absorption edge of g-C$_3$N$_4$ is 460 nm, indicating its small bandgap and good response to the visible light. While LaCO$_3$OH exhibits a light absorption edge of 300 nm, demonstrating its large bandgap along with poor visible light absorption capability. For g-C$_3$N$_4$/LaCO$_3$OH and RGO/g-C$_3$N$_4$/LaCO$_3$OH, light absorption edges are located at 475 and 500 nm respectively, indicating the improved visible light absorption capability benefiting from the construction of heterojunction and the introduction of cocatalyst RGO. The band gaps E_g (eV) of LaCO$_3$OH and g-C$_3$N$_4$ can be calculated based on the Kubelka–Munk function:

$$\alpha \hbar v = A(\hbar v - E_g)^{n/2} \qquad (1)$$
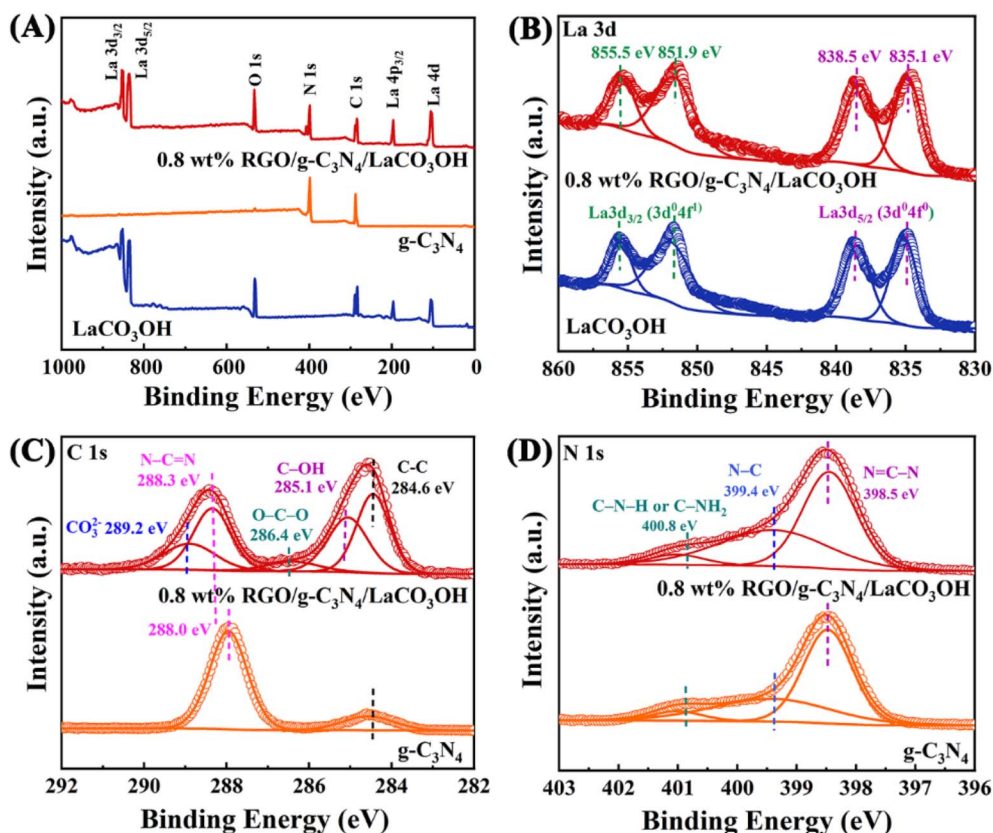
Fig. 2 XPS spectra of RGO/g-C$_3$N$_4$/LaCO$_3$OH: (A) the survey spectrum compared with g-C$_3$N$_4$ and LaCO$_3$OH; (B) La 3d spectrum compared with LaCO$_3$OH; (C) C 1s spectrum and (D) N 1s spectrum compared with g-C$_3$N$_4$.
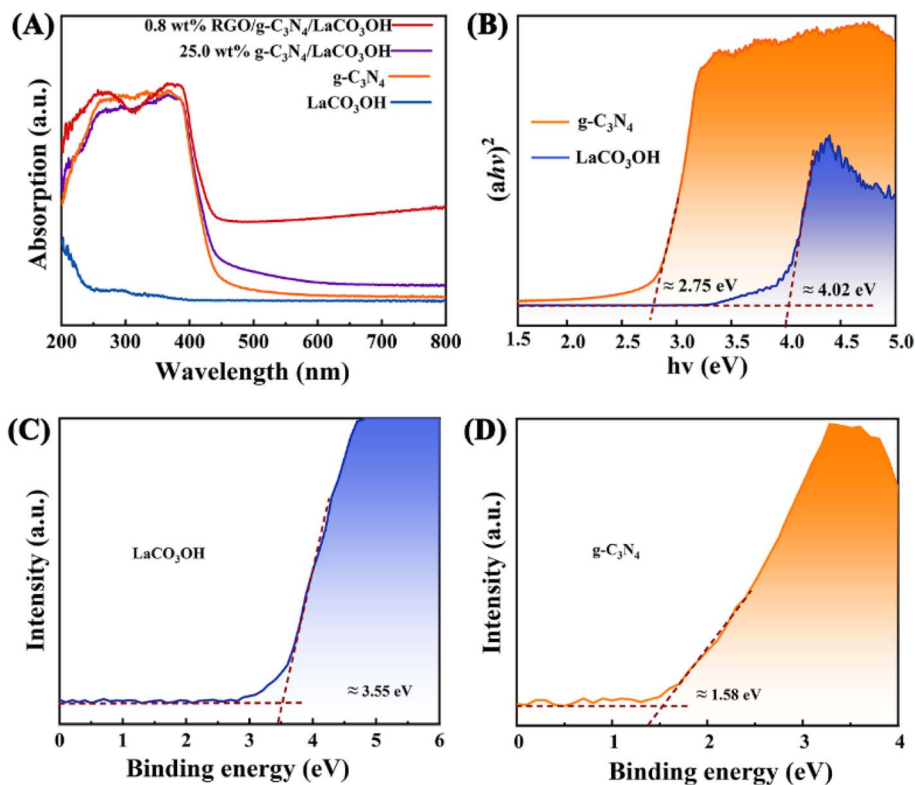
Fig. 3 (A) The UV–vis spectra of LaCO$_3$OH, g-C$_3$N$_4$, g-C$_3$N$_4$/LaCO$_3$OH and RGO/g-C$_3$N$_4$/LaCO$_3$OH; (B) the bandgap energy diagram and the valence band (XPS) spectra of the (C) LaCO$_3$OH and (D) g-C$_3$N$_4$.

where A, ν, $\hbar$ and α are constant, light frequency, Plank's constant and the absorption coefficient, respectively. For semiconductors such as g-C$_3$N$_4$ and LaCO$_3$OH, $n = 4$.[24] The calculated E_g for LaCO$_3$OH and g-C$_3$N$_4$ are 2.75 and 4.02 eV, respectively (Fig. 3B). According to the results of XPS spectra, the valence band (VB) potentials (E_{VB}) of LaCO$_3$OH and g-C$_3$N$_4$ can also be calculated. As shown in Fig. 3C and D, the results are 3.55 and 1.58 eV, respectively. The conduction band (CB) potentials (E_{CB}) can be calculated by the equation:

$$E_{CB} = E_{CB} - E_g \qquad (2)$$

The calculated E_{CB} of LaCO$_3$OH and g-C$_3$N$_4$ are 0.47 and −1.17 eV, respectively.

The photocatalytic performance of the obtained hetero-structured products were assessed by the photodegradation of MO under the visible light irradiation. After 50 min, the degradation of MO without catalysts is negligible, as shown in Fig. 4A. For pure LaCO$_3$OH, the photodegradation activity is low with a MO removal ratio of only 6.8% after 50 min because of its poor visible light absorption capability, which is proved by its UV–vis spectrum. Constructing g-C$_3$N$_4$/LaCO$_3$OH hetero-junction can significantly improve the MO removal ratio. Among the composites with different mass ratios of g-C$_3$N$_4$, 25% g-C$_3$N$_4$/LaCO$_3$OH exhibited the highest activity with a calculated photodegradation rate constant of 0.0150 min^{-1}

(Fig. 4B), which is 50.0 and 1.8 times higher than LaCO$_3$OH and g-C$_3$N$_4$ respectively. Such results confirmed that the construction of heterojunction could be conducive to the improvement of photocatalytic activity compared with each component.

Whereas, though the MO removal ratio has been effectively improved, the photodegradation of MO only 51.2%. To further improve the activity of the photocatalyst and shorten the reaction time, RGO was introduced into the composite as the cocatalyst. Photocatalytic performances of ternary RGO/g-C$_3$N$_4$/LaCO$_3$OH composite with different mass ratios of RGO is shown in Fig. 4C. Though RGO itself shows no activity in the photo-degradation of MO as expected, the introduction of RGO into 25% g-C$_3$N$_4$/LaCO$_3$OH can still further enhance its photo-catalytic performance. When the reaction time decreased to 50 min, the MO removal ratio of 0.8% RGO/g-C$_3$N$_4$/LaCO$_3$OH can be remarkably improved to 84.5%, which is the highest among ternary composites with different mass ratios, and is much improved compared with 25% g-C$_3$N$_4$/LaCO$_3$OH (51.2%). The corresponding photodegradation rate constant of 0.8% RGO/g-C$_3$N$_4$/LaCO$_3$OH is 0.0326 min^{-1}, which is 2.17 times higher than that of 25% g-C$_3$N$_4$/LaCO$_3$OH (Fig. 4D). Such improvement arises from the introduction of cocatalyst RGO, which can serve as the transfer medium for the photogenerated carriers, thus can accelerate their transfer kinetics and restrain their recombination, leading to an increased rate of photo-catalytic reaction.
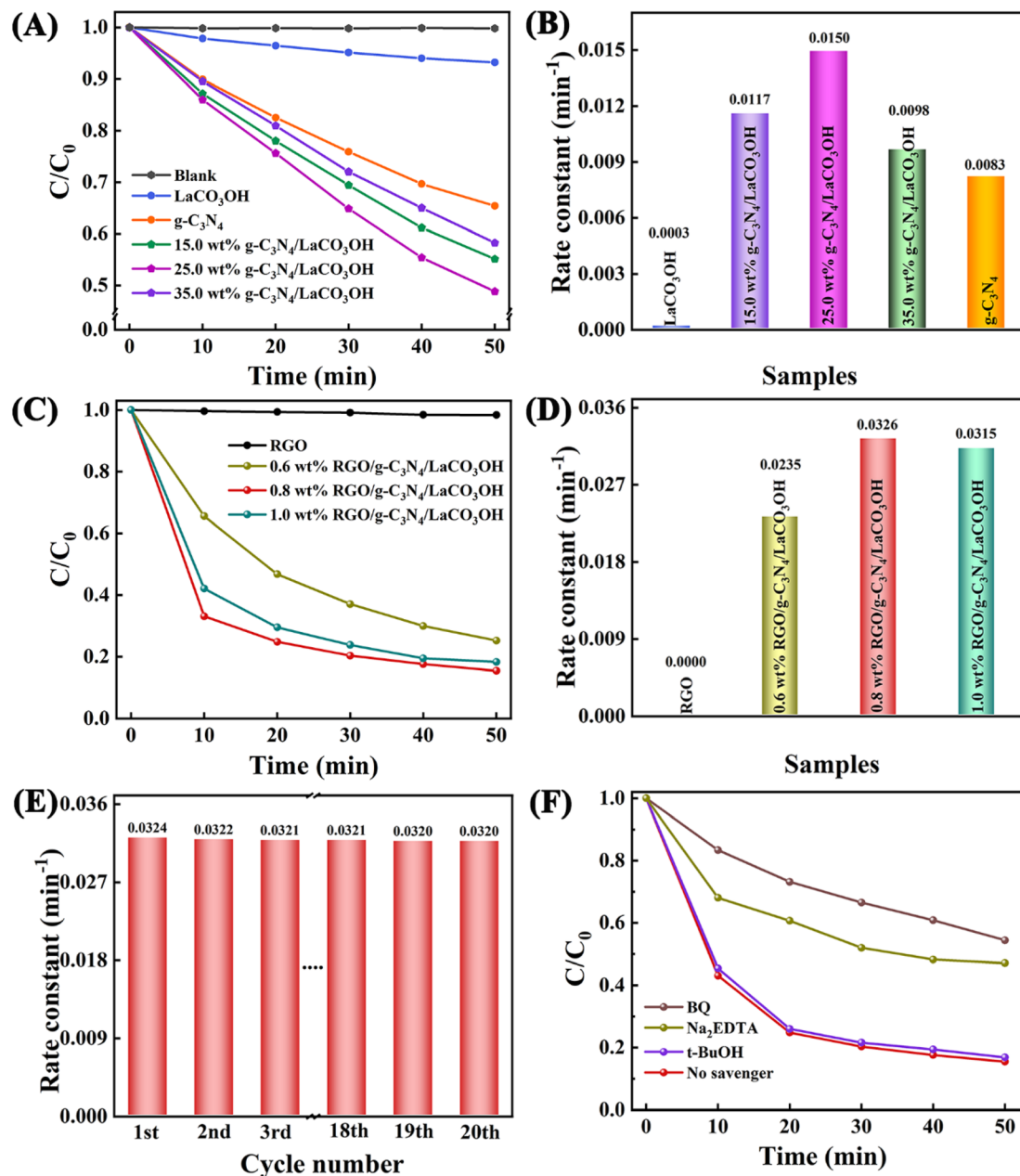
Fig. 4 (A) The activities of the MO photodegradation using RGO, g-C_3N_4, LaCO$_3$OH and g-C_3N_4/LaCO$_3$OH with different ratios of g-C_3N_4 as catalysts during 50 min and (B) the corresponding photodegradation rate constants; (C) the activities of the MO photodegradation using RGO and RGO/g-C_3N_4/LaCO$_3$OH with different ratios of RGO as catalysts during 50 min and (D) the corresponding photodegradation rate constants; (E) the cyclic tests and (F) activities of the MO photodegradation in the presence of three scavengers of 0.8% RGO/g-C_3N_4/LaCO$_3$OH.

The high stability of ternary RGO/g-C_3N_4/LaCO$_3$OH composite was clarified by the cycling test carried out using 0.8% RGO/g-C_3N_4/LaCO$_3$OH as the catalyst. As shown in Fig. 4E, the rate constant remains basically stable during 20 cycles. The slight decrease was generated by the sample loss during the washing and drying process after each cycle. TEM images shows that after the long-time cycling, there is no obvious change in the microstructure of the RGO/g-C_3N_4/LaCO$_3$OH composite, confirming its high structural stability (Fig. S2†). Moreover, the active species trapping experiment was taken to analyze the

active species during the photocatalytic degradation process (Fig. 4F). There is no significant change on MO removal ratio with the existence of *t*-BuOH, demonstrating that ˙OH radical does not involved in the photodegradation reaction. While with the addition of 1,4-benzoquinone (BQ) and Na$_2$EDTA, the MO removal ratio declined from 84.5% to 45.6% and 52.9% respectively, indicating that both active species ˙O_2^- and h$^+$ play a critical role in the photodegradation process. The above characterizations show that compared with single components, RGO/g-C_3N_4/LaCO$_3$OH exhibits an enhanced photocatalytic
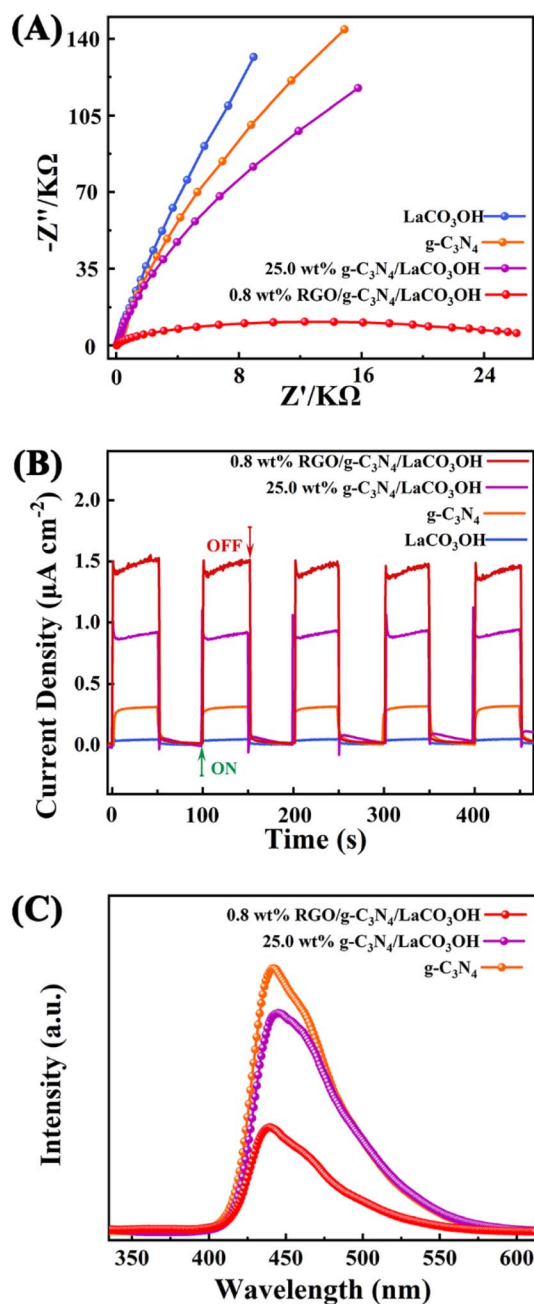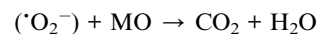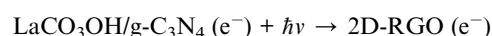
Fig. 5 (A) The Nyquist plots of RGO, g-C$_3$N$_4$, LaCO$_3$OH and RGO/g-C$_3$N$_4$/LaCO$_3$OH in the frequency range from 10^6 Hz to 0.1 Hz; (B) transient photocurrent responses and (C) the PL spectra.

activity for MO degradation, which is owing to the construction of heterojunction and the introduction of cocatalyst RGO.

More photoelectrochemical characterizations including EIS tests, transient photocurrent responses and PL spectroscopy were performed to study the separation efficiency of photo-generated charge carriers. The Nyquist plots (Fig. 5A) demonstrates that 0.8% RGO/g-C$_3$N$_4$/LaCO$_3$OH has the smallest semicircle radius in the high-frequency region compared with that of g-C$_3$N$_4$/LaCO$_3$OH, g-C$_3$N$_4$ and LaCO$_3$OH, indicating its lowest charge transfer resistance benefited from the

construction of the heterojunction and the introduction of RGO, leading to the highest separation efficiency of photo-generated electron–hole pairs.[26] Transient photocurrent curves during five on/off cycles are shown in Fig. 5B. 0.8% RGO/g-C$_3$N$_4$/LaCO$_3$OH generates a stable and highest photocurrent of 1.52 μA cm^{-2}, which is 1.78 and 4 times higher compared with 25% g-C$_3$N$_4$/LaCO$_3$OH (0.85 μA cm^{-2}) and g-C$_3$N$_4$ (0.38 μA cm^{-2}), indicating the heterostructured ternary composite can effectively accelerate the charge transfer process. In PL spectra, the lower PL intensity means the lower recombination rate and longer lifetime of the photogenerated carriers.[27] As shown in Fig. 5C, compared with g-C$_3$N$_4$ and 25% g-C$_3$N$_4$/LaCO$_3$OH, the PL intensity of 0.8% RGO/g-C$_3$N$_4$/LaCO$_3$OH is much lower, confirming that cocatalyst RGO plays an important role in the restriction of photogenerated carriers' recombination. Overall, the synergistic effect of heterostructure and cocatalyst RGO endows RGO/g-C$_3$N$_4$/LaCO$_3$OH composite an improved photo-catalytic activity by reducing the charge transfer resistance, facilitating the separation of charge carries and lowering their recombination rate.

According to above characterizations, the mechanism of the MO photodegradation process using RGO/g-C$_3$N$_4$/LaCO$_3$OH composite as the catalyst was proposed, as shown in Fig. 6. With the irradiation of visible light, g-C$_3$N$_4$ with a smaller bandgap of 2.75 eV can be excited and produce photogenerated electrons and holes, while LaCO$_3$OH does not response to visible light due to its large bandgap (4.02 eV). The electrons generated on the VB of g-C$_3$N$_4$ (1.58 eV) can be excited and separate with holes, then transfer to the CB of g-C$_3$N$_4$ (−1.17 eV). As g-C$_3$N$_4$ has a more negative CB compared with LaCO$_3$OH (−0.47 eV), the photogenerated electrons will transfer to the CB of LaCO$_3$-OH driven by the interfacial electric field force, thus the recombination of photogenerated electrons and holes can be retarded. The introduction of RGO as cocatalyst can not only enhance the light absorption efficiency but also provide abundant active sites for the photocatalytic reaction because of the enlarged surface area and facilitated charge transfer kinetics of RGO. The main reactions in the photodegradation process of MO are as follows:

$$g\text{-}C_3N_4 + \hbar v \rightarrow g\text{-}C_3N_4\ (h^+) + LaCO_3OH/g\text{-}C_3N_4\ (e^-)$$

$$LaCO_3OH/g\text{-}C_3N_4\ (e^-) + \hbar v \rightarrow 2D\text{-}RGO\ (e^-)$$

$$LaCO_3OH/g\text{-}C_3N_4\ (e^-) + 2D\text{-}RGO\ (e^-) + O_2 \rightarrow (\cdot O_2^-)$$

$$(\cdot O_2^-) + MO \rightarrow CO_2 + H_2O$$

$$g\text{-}C_3N_4\ (h^+) + MO \rightarrow CO_2 + H_2O$$
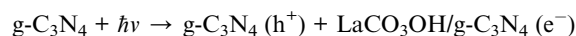
During this process, N=N bond of MO was broken under the attack of generated radicals, and aromatic hydrocarbons such as 4-amino-*N*,*N*-dimethylaniline and 4-diazenyl-*N*,*N*-dimethyl benzenamine were produced. Then the aromatic rings were continuously opened under the attack of reactive oxygen species and converted into carbon dioxide and water eventually.[28–30]
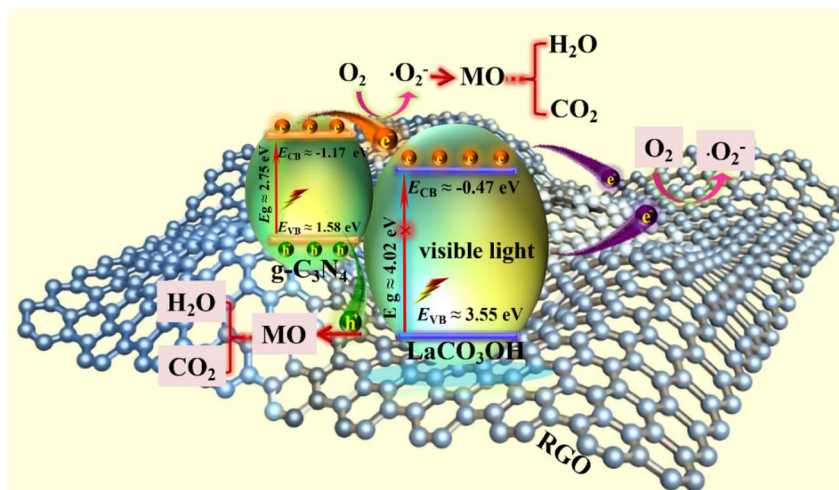
Fig. 6 The schematic of the proposed mechanism of RGO/g-C$_3$N$_4$/LaCO$_3$OH composites for MO photodegradation under visible light irradiation.

4. Conclusion

In summary, ternary RGO/g-C$_3$N$_4$/LaCO$_3$OH composite was constructed by coupling RGO with heterostructured g-C$_3$N$_4$/LaCO$_3$OH through a hydrothermal reaction, and serve as an effective catalyst for the photodegradation of MO under visible light. Compared with pure g-C$_3$N$_4$, the MO photo-degradation rate can be increased from 0.0083 min^{-1} to 0.0150 min^{-1} by constructing g-C$_3$N$_4$/LaCO$_3$OH hetero-junction, and further boosted to 0.0326 min^{-1} by introducing RGO as the cocatalyst, which is 3.93 times higher than pure g-C$_3$N$_4$. Such significant improvement is owing to the improved photocatalytic activities stemmed from the combination of g-C$_3$N$_4$/LaCO$_3$OH heterostructure with RGO, which can accelerate the transfer and restrict the recombination of the pho-togenerated carriers, and prolong their lifetime. This study realized the utilization of LaCO$_3$OH with a broad bandgap in the visible light region as a promising photocatalyst for the MO degradation, and also proposed a novel strategy for the further development of photocatalyst based on semi-conductors with wide bandgaps.

Conflicts of interest

There are no conflicts to declare.

Acknowledgements

References

1 J. Yang, D. Wang, H. Han and C. Li, *Acc. Chem. Res.*, 2013, **46**, 1900–1909.

2 Q. Z. Zhang, J. J. Deng, Z. H. Xu, M. Chaker and D. L. Ma, *ACS Catal.*, 2017, **7**, 6225–6234.

3 Z. Lei, W. You, M. Liu, G. Zhou, T. Takata, M. Hara, K. Domen and C. Li, *Chem. Commun.*, 2003, 2142–2143, DOI: **10.1039/B306813G**.

4 Y. Gao, J. Y. Lin, Q. Z. Zhang, H. Yu, F. Ding, B. T. Xu, Y. G. Sun and Z. H. Xu, *Appl. Catal., B*, 2018, **224**, 586–593.

5 C. Z. Zhu, Y. T. Wang, Z. F. Jiang, F. C. Xu, Q. M. Xian, C. Sun, Q. Tong, W. X. Zou, X. G. Duan and S. B. Wang, *Appl. Catal., B*, 2019, **259**, 118072.

6 T. Lv, Z. N. Xu, W. Hong, G. F. Li, Y. W. Li and L. S. Jia, *Chem. Eng. J.*, 2020, **382**, 123021.

7 Y. Gao, C. Shi, J. Z. Feng, G. Y. Zhao, H. Yu, Y. F. Bi, F. Ding, Y. G. Sun and Z. H. Xu, *RSC Adv.*, 2017, **7**, 54555–54561.

8 Z. H. Xu, M. Quintanilla, F. Vetrone, A. O. Govorov, M. Chaker and D. L. Ma, *Adv. Funct. Mater.*, 2015, **25**, 2950–2960.

9 Y. Lin, W. Su, X. Wang, X. Fu and X. Wang, *Angew. Chem., Int. Ed.*, 2020, **59**, 20919–20923.

10 Y. Gao, B. T. Xu, M. Cherif, H. Yu, Q. Z. Zhang, F. Vidal, X. F. Wang, F. Ding, Y. G. Sun, D. L. Ma, Y. F. Bi and Z. H. Xu, *Appl. Catal., B*, 2020, **279**, 119403.

11 B. L. Li, L. L. Li and C. Zhao, *Green Chem.*, 2017, **19**, 5412–5421.

12 B. Pan, Q. Xie, H. Wang, J. Zhu, Y. Zhang, W. Su and X. Wang, *J. Mater. Chem. A*, 2013, **1**, 6629–6634.

13 Z. Wang, Y. Huang, L. Chen, M. Chen, J. Cao, W. Ho and S. C. Lee, *J. Mater. Chem. A*, 2018, **6**, 972–981.

14 B. Pan, Q. H. Xie, H. M. Wang, J. Zhu, Y. F. Zhang, W. Y. Su and X. X. Wang, *J. Mater. Chem. A*, 2013, **1**, 6629.

15 S. S. Patil, M. G. Mali, A. Roy, M. S. Tamboli, V. G. Deonikar, D. R. Patil, M. V. Kulkarni, S. S. Al-Deyab, S. S. Yoon,

S. S. Kolekar and B. B. Kale, *J. Energy Chem.*, 2016, **25**, 845–853.

16 Z. Y. Wang, Y. Huang, L. Chen, M. J. Chen, J. J. Cao, W. K. Ho and S. C. Lee, *J. Mater. Chem. A*, 2018, **6**, 972–981.

17 Y. Gao, K. Qian, B. T. Xu, F. Ding, V. Dragutan, I. Dragutan, Y. Sun and Z. Xu, *RSC Adv.*, 2020, **10**, 32652–32661.

18 X. Feng, H. Chen, F. Jiang and X. Wang, *Chem. Eng. J.*, 2018, **347**, 849–859.

19 B. Pan, S. Luo, W. Su and X. Wang, *Appl. Catal., B*, 2015, **168–169**, 458–464.

20 J. X. Li, C. Ye, X. B. Li, Z. J. Li, X. W. Gao, B. Chen, C. H. Tung and L. Z. Wu, *Adv. Mater.*, 2017, **29**, 1606009–1606014.

21 M. Xiao, L. Zhang, B. Luo, M. Lyu, Z. Wang, H. Huang, S. Wang, A. Du and L. Wang, *Angew. Chem., Int. Ed.*, 2020, **59**, 7230–7234.

22 Q. H. Zhu, Z. H. Xu, B. C. Qiu, M. Y. Xing and J. L. Zhang, *Small*, 2021, **17**, 2101070–2101095.

23 S. D. Perera, R. G. Mariano, K. Vu, N. Nour, O. Seitz, Y. Chabal and K. J. Balkus, *ACS Catal.*, 2012, **2**, 949–956.

24 Z. H. Xu, B. T. Xu, K. Qian, Z. Li, F. Ding, M. Fan, Y. Sun and Y. Gao, *RSC Adv.*, 2019, **9**, 25638–25646.

25 Y. Fu, J. Zhu, C. Hu, X. Wu and X. Wang, *Nanoscale*, 2014, **6**, 12555–12564.

26 Z. H. Xu, M. G. Kibria, B. AlOtaibi, P. N. Duchesne, L. V. Besteiro, Y. Gao, Q. Z. Zhang, Z. Mi, P. Zhang, A. O. Govorov, L. Q. Mai, M. Chaker and D. L. Ma, *Appl. Catal., B*, 2018, **221**, 77–85.

27 Z. P. Wang, Z. L. Wang, X. D. Zhu, C. Z. Ai, Y. M. Zeng, W. Y. Shi, X. D. Zhang, H. R. Zhang, H. W. Si, J. Li, C. Z. Wang and S. W. Lin, *Small*, 2021, **17**, 2102699–2102710.

28 S. Balasurya, M. K. Okla, I. A. Alaraidh, A. A. Al-ghamdi, A. Mohebaldin, M. A. Abdel-Maksoud, R. F. Abdelaziz, A. M. Thomas, L. L. Raju and S. S. Khan, *J. Environ. Manage.*, 2022, **319**, 115674.

29 Z. Zhang, G. Wang, W. Li, L. Zhang, T. Chen and L. Ding, *Colloids Surf., A*, 2020, **601**, 125034.

30 V. Subhiksha, A. A. Alatar, M. K. Okla, I. A. Alaraidh, A. Mohebaldin, M. Aufy, M. A. Abdel-Maksoud, L. L. Raju, A. M. Thomas and S. S. Khan, *Chemosphere*, 2022, **303**, 135177.